In-situ multi-step pulsed vapor phase surface functionalization of zirconia nanoparticles *via* copper-free click chemistry

Iva Šarić,[a,b] Maria Kolympadi Markovic,[a,b] Robert Peter,[a,b] Petra Linić,[c] Karlo Wittine,[c] Ivna Kavre Piltaver,[a,b] Ivana Jelovica Badovinac,[a,b] Dean Marković,[c] Mato Knez,[d,e]* Gabriela Ambrožić [a,b]*

[a]Department of Physics, University of Rijeka, Radmile Matejčić 2, 51000 Rijeka, Croatia

[b]Centre for Micro- and Nanosciences and Technologies, University of Rijeka, Radmile Matejčić 2, 51000 Rijeka, Croatia

[c]Department of Biotechnology, University of Rijeka, Radmile Matejčić 2, 51000 Rijeka, Croatia

[d]CIC nanoGUNE, 20018 San Sebastian, Spain

[e]IKERBASQUE, Basque Foundation for Science, 48013 Bilbao, Spain

*E-mail: gabriela.ambrozic@uniri.hr

Phone: (+385)51-584-632

Abstract

We report on multi-step copper-free vapor phase azide-alkyne click reactions for the functionalization of metal oxide nanopowders, automated with the atomic layer deposition (ALD) technique. The synthetic approach consists of the following reaction steps: chemisorption of propiolic acid (PA) to ZrO_2 from the gas phase, followed by the formation of a triazole ring through a click reaction with 1,4-bis(azidomethyl)benzene (BisA), and, in the final step, click-coupling of the pendant azide groups with a second dose of propiolic acid (PA). The chemical composition and nature of the chemical bonding in the samples obtained after each of the ALD processing steps were investigated in detail by ATR-FTIR and XPS. As confirmed by an additional ALD deposition of ZnO, the latter reaction step introduces free polar carboxylic acid functionalities to the nanomaterial surface, which enhance the stability of the chemically modified zirconia in ethanolic dispersion. This proof-of-concept study offers great potential toward the fabrication of functional organic layers on metal oxide surfaces by sequential azide-alkyne cycloadditions performed in ALD.

Keywords: azide-alkyne click chemistry, atomic layer deposition, molecular layer deposition, zirconia nanoparticles, ATR-FTIR, XPS.

1. Introduction

A simultaneous presence of organic and inorganic materials in a nanostructure is a very promising approach for extending the range of functionalities of nanomaterials. Typically, chemical approaches to introduce specific organic moieties to the surfaces of metal oxide substrates are investigated for the purpose of optimizing and/or creating new physicochemical properties [1, 2]. For instance, the chemical binding of appropriate organic moieties onto ceramic surfaces can impart desired functionalities, such as selective bio-recognition or biocompatibility, stimuli-responsiveness, enhanced catalytic activity, etc.

The vast majority of surface functionalization strategies of metal oxides rely on wet chemical methods, starting with an initial binding of functional molecules, mostly through phosphonate, carboxylate or silane anchoring functionalities. After successful grafting of such reactive species, various reactions are applied to couple new molecules to the pre-functionalized surfaces. Among the post-modification reactions, the Cu-catalyzed Huisgen cycloaddition (CuAAC) [3] is excellent for grafting a wide variety of low or high molar-mass molecules onto ceramic surfaces [4-6]. It involves a highly selective coupling of azides and alkynes, yielding stable triazole rings without undesired byproducts. However, despite its selectivity, the wet chemical CuAAC has some limitations, especially concerning possible contaminations of the inorganic surfaces with copper (II) catalyst residues or reducing agents. Moreover, less volatile polar solvents, e.g. water, may physisorb on the surface of polar substrates. Avoiding the use of catalysts and solvents is highly desirable. It may reduce contamination and improve the functionality of the materials and the fabrication routes.

Inducing organic reactions on solid substrates from the vapor-phase is an alternative pathway and has been investigated for functionalization of metal oxides [7-9]. Typically, this proceeds *via* direct coupling of organic vapors to a solid substrate without the need of mediation of solvents and/or a catalyst. Nonetheless, when compared to the plethora of possible variations of reactants and reaction conditions available in “classical” wet chemistry, vapor chemistry is still in its infancy and much remains to be understood and explored. Among vapor phase processes, atomic layer deposition (ALD) and molecular layer deposition (MLD), have emerged as highly versatile tools for depositing thin inorganic, organic or hybrid organic-inorganic films on a great variety of substrates [10, 11]. Unlike other chemical vapor phase processes, such as chemical vapor deposition (CVD), ALD and MLD provide vaporized metal-organic (ALD) and/or organic (MLD) precursors and co-reactants to a substrate in an alternating fashion. The vapors react with active surface groups of the substrate in a cyclic

repetition, each time saturating, self-terminating and restoring the surface for the next cycle. In this way, the stepwise growth of a thin film is obtained with a thickness control as a function of the number of repetitive cycles. However, the limited number of investigated reactions, the lack of an adequate number of organic reactants exhibiting sufficient thermal stability under low pressure, and, finally, the poor understanding of the reactivity of vaporized organic molecules are some of the challenges, as well as opportunities, for developing functional hybrid materials by ALD/MLD processes.

In our previous work, we have shown that the ALD setup can serve as an automated vacuum vapor phase processing method for an efficient and time-effective modification of metal oxides through the copper-free click coupling of benzyl azide to propiolic acid (PA) [12]. The benefit of using the ALD setup for developing our model system relied on an *in-situ* process with two distinct reactions, i.e. non-etching surface attachment of PA to ZnO, followed by a selective click reaction between free ethynyl groups on ZnO and benzyl azide, thus avoiding any additional isolation and/or purification step of the intermediate hybrid product.

Herein, we expand our previous research and investigate the pulsed vapor phase click azide-alkyne reactions for building larger bis-triazole organic monolayers on ZrO_2 from propiolic acid (**1**) (PA) and 1,4-bis(azidomethyl)benzene (**2**) (BisA) as precursors (**Scheme 1**). Commercially available zirconia powder consisting of nanoparticles with an average particle size of cca. 20 nm was used as a substrate in the present study (see **Fig. S1** in the Supporting material). The *homo*-bifunctional organic precursor BisA, synthesized by azidation of 1,4-bis(bromomethyl)benzene (see **Scheme S1** in the Supporting material), was chosen as an organic precursor, because its central aromatic ring was expected to prevent bending of the molecule and thus unwanted double reactions of two azide groups with the surface, a phenomenon generally seen when longer aliphatic bifunctional molecules are used as MLD precursors [13]. Additionally, BisA fulfills the criteria of thermal stability and sufficient vapor pressure, which are lifelines for feasible ALD processes. BisA is a low melting point solid (m.p. 30- 32 ºC), but it volatilizes when heated at medium-high pressures (b.p. 82- 83 °C, 0.1 Torr) [14]. Furthermore, the compound is thermally stable even if exposed to multiple heating-cooling cycles upon performing several ALD experiments.

Scheme 1 presents our proposed three-step reaction sequence consisting of: i) initial gas-phase chemisorption of PA to ZrO_2 yielding an ethynyl-terminated surface (sample **ZrO_2/PA**), ii) formation of a triazole ring through a click-reaction of the PA-modified ZrO_2 with BisA vapors (sample **ZrO_2/PA/BisA**) generating an azide-terminated surface, and iii) click-coupling between the pendant azide groups of **ZrO_2/PA/BisA** and PA vapors (sample

ZrO_2/PA/BisA/PA). The introduction of free carboxylic functionalities on nanomaterial surfaces through pulsing of PA in the third reaction step is especially interesting from a point-of-view of ligand engineering, as these groups can impart desired properties, such as hydrophilicity of organic layers [15], or reactivity towards metal ions [16] or amine residues on biomolecules, the latter being useful for bio-sensing or bioimaging applications [17, 18]. The ALD parameters (pulse-purge durations, temperatures of the chamber and precursor containers) were explored in detail in order to obtain optimal conditions for the most effective click-chemistry reactions for this particular multi-step system. Moreover, a comparison with the corresponding wet chemical pathway was attempted after applying a pre-synthesized dicarboxylic acid to zirconia, revealing the utility of pulsed vapor phase process for the surface modification of metal oxides.

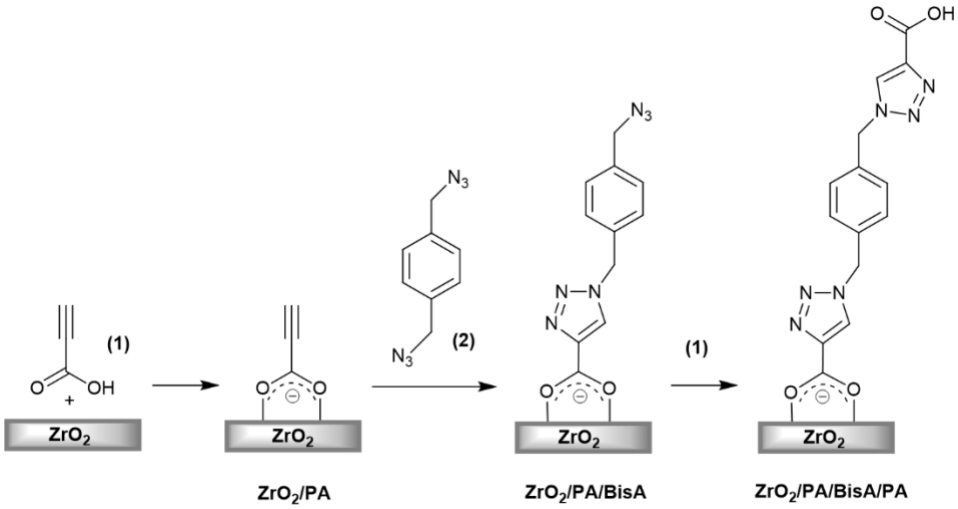

Scheme 1. Pulsed vapor phase surface modification process of zirconia in three steps using propiolic acid **(1)** (PA) and 1,4-bis(azidomethyl)benzene **(2)** (BisA) as organic precursors. Note that the growth does not involve cross-linking of the molecules.

2. Materials and Methods

2.1 Materials

Propiolic acid (98 %), sodium azide (99 %), 1,4-bis(bromomethyl)benzene (97 %), copper(II) sulfate pentahydrate (99 %), and sodium L-ascorbate (99 %) were purchased from Acros Organics. ZrO_2 nanopowder (~ 20 nm particle size), *N*,*N*-dimethylformamide (DMF) (puriss

p.a.) and absolute ethanol (puriss p.a.) were obtained from Sigma-Aldrich, while diethylzinc (DEZ, ≥ 95 %) was purchased from Strem Chemicals. All chemicals were used as received.

2.2. Synthesis of materials

2.2 1. ALD processing

ZrO_2 nanopowder was mixed with a minimum amount of absolute ethanol under ultrasound agitation in order to form a stable and homogeneous paste. It was then drop casted on clean silicon wafer pieces and allowed to dry in air. The substrates for ALD processing were additionally kept in the ALD reactor for 2 hours at a temperature of 130 ºC before processing. Vapor phase modification was carried out using a Cambridge Nanotech Savannah S100 atomic layer deposition tool. Nitrogen (≥ 99.99 % N_2) was used as the delivery and purge gas. During the processing, the pressure in the reaction chamber was maintained at 0.75 Torr, and all gas lines were kept at 120 ºC to avoid cold spots and condensations of the precursors. Chemical functionalization of the ZrO_2 surface with PA and BisA was carried out at a processing temperature of 130 ºC. Optimum *in-situ* three-step pulsed vapor phase surface modification conditions for the investigated click reaction were performed by applying the following pulsing/exposure/purging sequences: a) 40 pulses of PA (4 s each), 30 s exposure of the substrate to PA, 120 s N_2 purge (intermediate sample **ZrO_2/PA**), 390 pulses of Bis A (4 s each), 30 s exposure of the substrate to BisA, 120 s N_2 purge (intermediate sample **ZrO_2/PA/BisA**), and 255 pulses of PA (4 s each), 30 s exposure of the substrate to PA, and 120 s N_2 purge (final sample **ZrO_2/PA/BisA/PA**). The PA and BisA containers were kept at room temperature and 120 ºC, respectively.

After chemical surface modification of the ZrO_2 surface with the three-step process described above, a ZnO deposition was performed at 50 °C applying 30 ALD cycles of Et_2Zn/water. One pulsing cycle consisted of: Et_2Zn pulsing (350 ms), N_2 purging (4 s), water pulsing (250 ms), N_2 purging (3 s). The deposition of ZnO was carried out with a Beneq TFS-200 ALD system under vacuum (0.1 mbar). The precursors were kept at 20 °C. After ALD processing, all samples were immediately transferred and stored in a desiccator under vacuum until further use.

*2.2.2. Synthesis of 1,4-bis(azidomethyl)benzene (**2**)* (BisA)

Sodium azide (6.00 g, 91.5 mmol) was added to a solution of 1,4-bis(bromomethyl)benzene (4.00 g, 14.8 mmol) in DMF (24 mL) and the mixture was heated at 60 °C under stirring overnight. After cooling to room temperature, water (70 mL) was added, and it was extracted

with diethylether (70 mL × 3). The combined organic layers were dried over anhydrous sodium sulfate, condensed under vacuum (CAREFUL DRYING UNDER MEDIUM VACUUM), and purified by column chromatography (silica gel, petroleum ether 40-60 °C) to afford **2** as a colorless oil (2.62 g, 94 %), which solidified at room temperature. ATR-FTIR (neat): $\tilde{\nu}$/cm^{-1} 3050 (very weak, aromatic C-H stretching), 2915 and 2848 (weak, aliphatic C-H stretching), 2090 (very strong, N=N=N asymmetric stretching), 1248 (medium, N=N symmetric stretching); ^{1}H NMR: (600 MHz, d_6-DMSO): δ/ppm 7.41 (s, 4H, C-H of phenyl, 4.47 (s, 4H, two CH_2). Spectroscopic data are in full agreement with literature [19].

*2.2.3 Synthesis of 1,1'-[1,4-phenylenebis(methylene)]bis(1H-1,2,3-triazole-4-carboxylic acid (**3**)*

Propiolic acid (**1**) (0.113 mL, 0.129 g, 1.84 mmol) was added to a solution of 1,4-bis(azidomethyl)benzene (**2**) (0.058 g, 0.31 mmol) in DMF (1 mL), followed by copper(II) sulfate pentahydrate (0.0033 g, 0.01 mmol) and sodium ascorbate (0.021 g, 0.11 mmol). The mixture was heated at 60 °C under stirring for 3 h. After cooling to room temperature, aqueous HCl 0.1 M (3 mL) was added and let overnight. The produced solid was separated by centrifugation (14000 rpm, 10 min), washed several times with aqueous HCl 0.1 M, demineralized water and dichloromethane, and dried under vacuum to afford **3** as a white solid (0.082 g, 95 %). m.p. 221- 223 ºC; ATR-FTIR (neat): $\tilde{\nu}$/cm^{-1} 3400- 2400 (very broad, H-bond associated OH stretching of carboxylic acid), 3115 (medium sharp, unassociated OH), 1678 (very strong, C=O stretching of conjugated carboxylic acid, H-bond associated dimer), 1541 (medium, C=C stretching), 1425 (medium, C-N and C-O-H in-plane bending), 1233 (strong, N=N stretching and C-O stretching), 1050 (strong, aromatic C-H in-plane bending), 945 (medium), 894 (medium), 784 (strong, C-H bending), 750 (medium, C-H bending); ^{1}H NMR (600 MHz, d_6-DMSO): δ/ppm 13.08 (s, 2H, 2× COOH), 8.76 (s, 2H, 2× C-H of triazole rings), 7.36 (s, 4H, C-H of phenyl ring), 5.64 (s, 4H, 2× CH_2); ^{13}C NMR (150 MHz, *d6*-DMSO): δ/ppm 162.0 (COOH), 140.4 and 136.1 (quartenary carbons), 129.5 (C-H of triazole rings), 128.9 (phenyl C-H), 53.1 (CH_2).

*2.2.4. Solution-phase grafting of ZrO_2 with **3***

20 µL of a solution of 1 mM dicarboxylic acid **3** in DMF was drop casted on a ZrO_2 substrate. It was dried under vacuum at 80 °C for 2 h and immediately stored in a desiccator under vacuum until analysis.

2.3. Characterization

Attenuated total reflection Fourier transform infrared (ATR-FTIR) spectroscopy was performed in the range of 4000 to 600 cm^{-1} at room temperature in air with a PerkinElmer Frontier FTIR spectrometer. All the spectra were obtained with a resolution of 4 cm^{-1} and 30 scans per spectrum with air as background.

X-ray photoemission spectroscopy (XPS) was carried out on a SPECS instrument equipped with a monochromatized source of Al Kα X-rays of 1486.74 eV and a hemispherical electron analyzer (Phoibos MCD 100). Spectra around the C 1s state were recorded at a pass energy of 10 eV, and spectra around the N 1s level were taken at a pass energy of 25 eV with the total acquisition time of 60 minutes. For monitoring of azide decomposition, the N 1s spectra were recorded at a pass energy of 50 eV, and the accumulated scans were measured at the same spot of the sample after 1, 10 and 20 minutes. The typical pressure in the UHV chamber during the XPS analysis was in the 10^{-9} Torr range. The spectra were analyzed by the Unifit software and simulated with several sets of mixed Gaussian-Lorentzian functions, while the background was subtracted according to the Shirley's method. All spectra were calibrated by setting the characteristic C 1s peak at the binding energy of 285.0 eV.

Nuclear magnetic resonance (NMR) spectra were recorded with a Bruker Avance 600 MHz and calibrated according to the solvent peak of d_6-DMSO: δ 2.50 ppm for ^{1}H and 39.5 ppm for ^{13}C.

3. Results and Discussion

Fig. 1 shows a comparison of ATR-FTIR spectra of the sample after each individual ALD processing step in the most significant spectral regions of a) 2200-1000 cm^{-1}, and b) 3400-3000 cm^{-1}. The ATR-FTIR spectrum acquired after the initial exposure of ZrO_2 to PA vapors (**ZrO_2/PA** in **Fig. 1a and 1b**) shows intense bands centered at 1567 and 1424 cm^{-1}, corresponding to asymmetric and symmetric stretching vibrations of carbonyl from the resonance-stabilized bidentate carboxylate of PA, respectively. An additional peak can be seen at 1615 cm^{-1} likely being minor contributions of the C=O stretching vibration in symmetry-breaking monodentate coordination of the carboxylate to zirconia [20, 21]. The peaks at 2114 (see magnification in **Fig. 1a**) and 3320 cm^{-1}, characteristic of -C≡C- and C≡C-H stretching vibrations, respectively, undoubtedly confirm that the coordination of the gas-phase PA generates free alkyne functionalities on the zirconia surface.

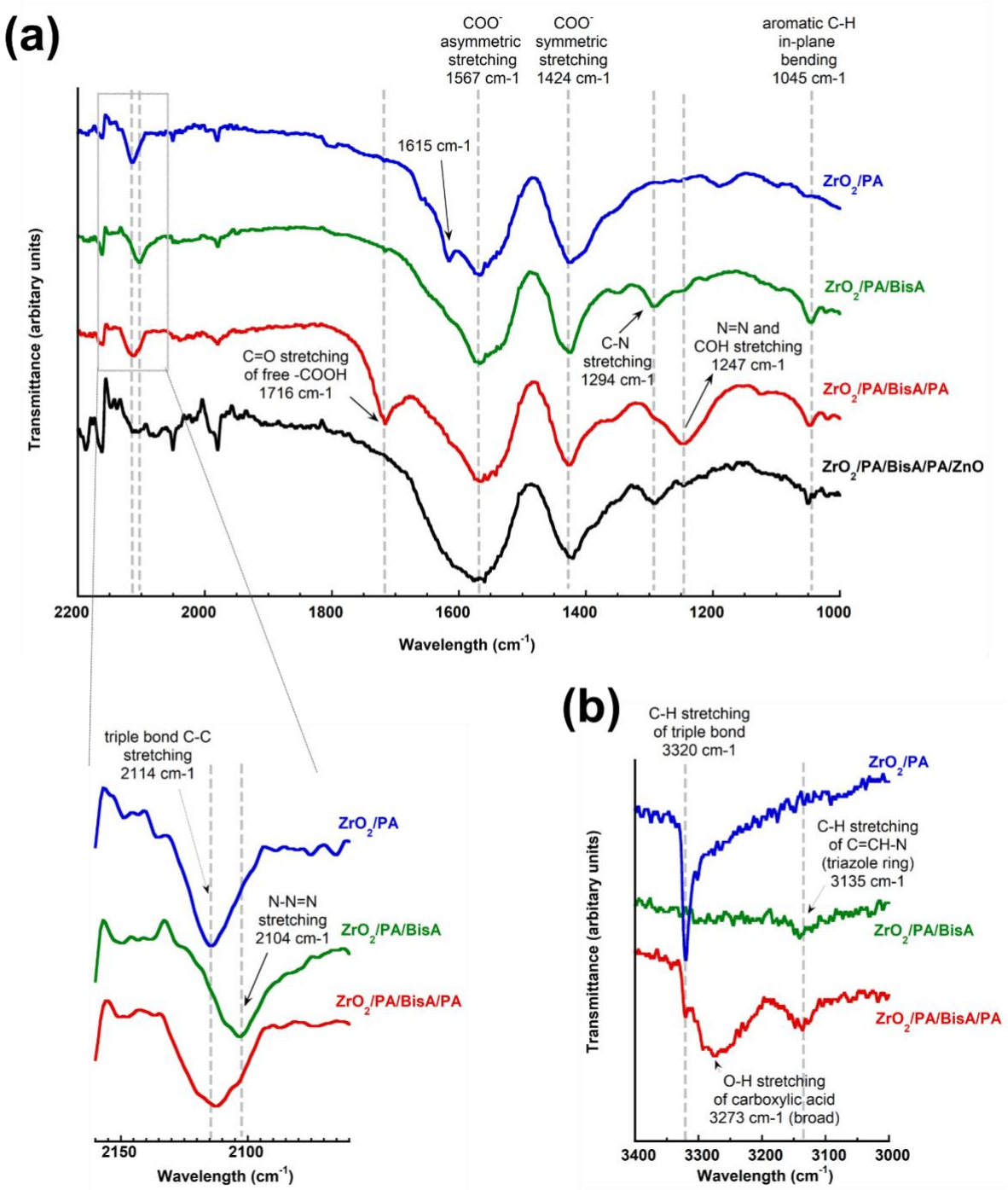

Fig. 1. ATR-FTIR spectra of: (a) **ZrO_2/PA**, **ZrO_2/PA/BisA**, **ZrO_2/PA/BisA/PA** and **ZrO_2/PA/BisA/PA/ZnO** in the 2200-1000 cm^{-1} region (the magnification around 2100 cm^{-1} shows the characteristic peaks of alkyne and azide functionalities); and (b) representative vibration bands of **ZrO_2/PA**, **ZrO_2/PA/BisA**, **ZrO_2/PA/BisA/PA** in the 3400-3000 cm^{-1} region. All spectra are normalized to the Zr-O band at 745 cm^{-1}.

Although in the ATR-FTIR spectrum of **ZrO_2/PA/BisA** the C=N stretching vibration of the triazole ring at approximately 1410 cm^{-1} cannot be seen due to the overlapping with the intense COO^- stretching bands of bound PA [12], some additional spectral features confirm the successful occurrence of the click reaction (**Fig. 1a** and **1b**). Namely, the new signals appearing at 1294 and 3135 cm^{-1} are assigned to -C–N- and N=C-H stretching vibrations of triazole formed upon successful click reaction [22, 23], respectively, while the peak at 1045 cm^{-1} can be ascribed to aromatic C-H in-plane bending of bound BisA [24]. A significant decrease in intensity of the -C≡CH stretching band from PA at 2114 cm^{-1} indicates the consumption of these groups as a consequence of the coupling with BisA. In addition, a new signal emerges at 2104 cm^{-1} representing the stretching vibration of $–N_3$. The presence of this peak shows that the vapor-phase reaction of BisA with PA-modified ZrO_2 occurs through only one of two azido groups present in BisA, suggesting that no double reactions of the bifunctional BisA with the ethynyl surface groups take place.

In the following reaction step, **ZrO_2/PA/BisA** was exposed to a second dose of PA vapors. Besides the intensity decrease of the azide stretching signal at 2104 cm^{-1} and the presence of intensive carboxylate bands, the ATR-FTIR spectrum of the obtained product **ZrO_2/PA/BisA/PA** shows a new signal at 1716 cm^{-1} and a broad band at 3273 cm^{-1}, coinciding with the C=O and O-H stretching vibrations of monomeric (not H-bound) COOH groups in carboxylic acids [25, 26]. These spectral features support the occurrence of a second click reaction between the alkyne functionality in PA and the pendant azide groups on the **ZrO_2/PA/BisA** substrate, which results in a COOH termination of the surface. A noticeable increase in intensity of the -C≡CH peak at 2114 cm^{-1} indicates a competing reaction, the direct attachment of PA to some available reactive sites on the zirconia surface through carboxylic acid groups, similar to the case of the initial (first-step) ALD exposure of zirconia to PA vapors. In previous results on PA-modified ZnO powder, the applied temperature of 130 ºC throughout the ALD process was identified to induce a partial desorption of PA, which leaves behind free active sites on ZnO [12]. Here, the process proceeds in analogy on zirconia substrates and the desorption generates active sites, which become accessible for subsequent binding of PA in the third processing step.

In order to provide a further proof for the presence of terminal carboxylic groups, **ZrO_2/PA/BisA/PA** was used as a substrate for an ALD deposition of ZnO. It is known that a coupling between carboxylic acid groups on a substrate and metal-organic vapors in ALD processes occurs through the initial formation of metal carboxylates [27, 28]. Therefore, a control ALD experiment based on exposing **ZrO_2/PA/BisA/PA** to Et_2Zn/H_2O pulses could

indirectly confirm the presence of free -COOH functionalities in the pristine sample. Indeed, the ATR-FTIR spectrum after the ZnO deposition (**ZrO_2/PA/BisA/PA/ZnO** in **Fig. 1a)** indicates the formation of $–COO^-$ groups represented by two spectral features: the disappearance of the C=O stretching vibration from COOH, and the broadening of the symmetric and asymmetric metal-carboxylate bands. Consequently, these ATR-FTIR results further confirm the successful formation of terminal COOH in the three-step gas-phase synthesis of **ZrO_2/PA/BisA/PA**.

XPS spectroscopy was used to provide further insight into the surface chemistry of the samples after each of the ALD processing steps. The C 1s and N 1s spectra of the samples are shown in **Fig. 2a** and **2b**, respectively. After the initial exposure to PA vapors, the deconvoluted C 1s spectrum of **ZrO_2/PA** exhibits three peaks (**Fig. 2a** top). The components at binding energies (BE) of 284.5 eV and 288.4 eV originate from the two different types of carbon atoms in the zirconia-bound PA, namely the ethyne group (sp hybridized C-C bonds) and the surface carboxylate group (C=O peak), respectively. Their relative ratio is approximately 2:1, as it is expected from the carbon content in the C≡C and COO^- groups, and is in agreement with the previous reports on ZnO substrates [12]. The additional C 1s peak (C-O peak) results from carbon contamination upon short exposure to ambient air or minor X-ray damage of COO^- groups. The subsequent click reaction with BisA featured an important change in the intensity of the C 1s core levels (**Fig. 2a**, middle). Namely, following the second reaction step, the components at 286.5 eV (C-N/C-O) and 284.5 eV (sp^2 and sp^3 hybridized C-C bonds) in **ZrO_2/PA/BisA** increase significantly with respect to the peak of C=O at 288.4 eV. These peaks are associated with the newly formed triazole bonds and aromatic carbons deriving from the coupled BisA, respectively.

Fig. 2b (top) shows the XPS spectrum of the N 1s region of **ZrO_2/PA/BisA.** The appearance of a broad peak at around 400 eV proves the presence of nitrogen atoms upon exposure of **ZrO_2/PA** to BisA vapors. Note that we also performed a control ALD experiment by exposing neat ZrO_2 to BisA vapors under the same processing conditions. In this case, no evidence of physisorption or chemisorption of BisA onto zirconia was observed by neither ATR-FTIR (not shown here) nor XPS (see N 1s spectral region in **Fig. 2b**, middle). This strongly suggests that the nitrogen in the **ZrO_2/PA/BisA** sample solely derives from the covalent coupling of BisA to the surface anchoring ethyne group *via* the indicated click reaction.

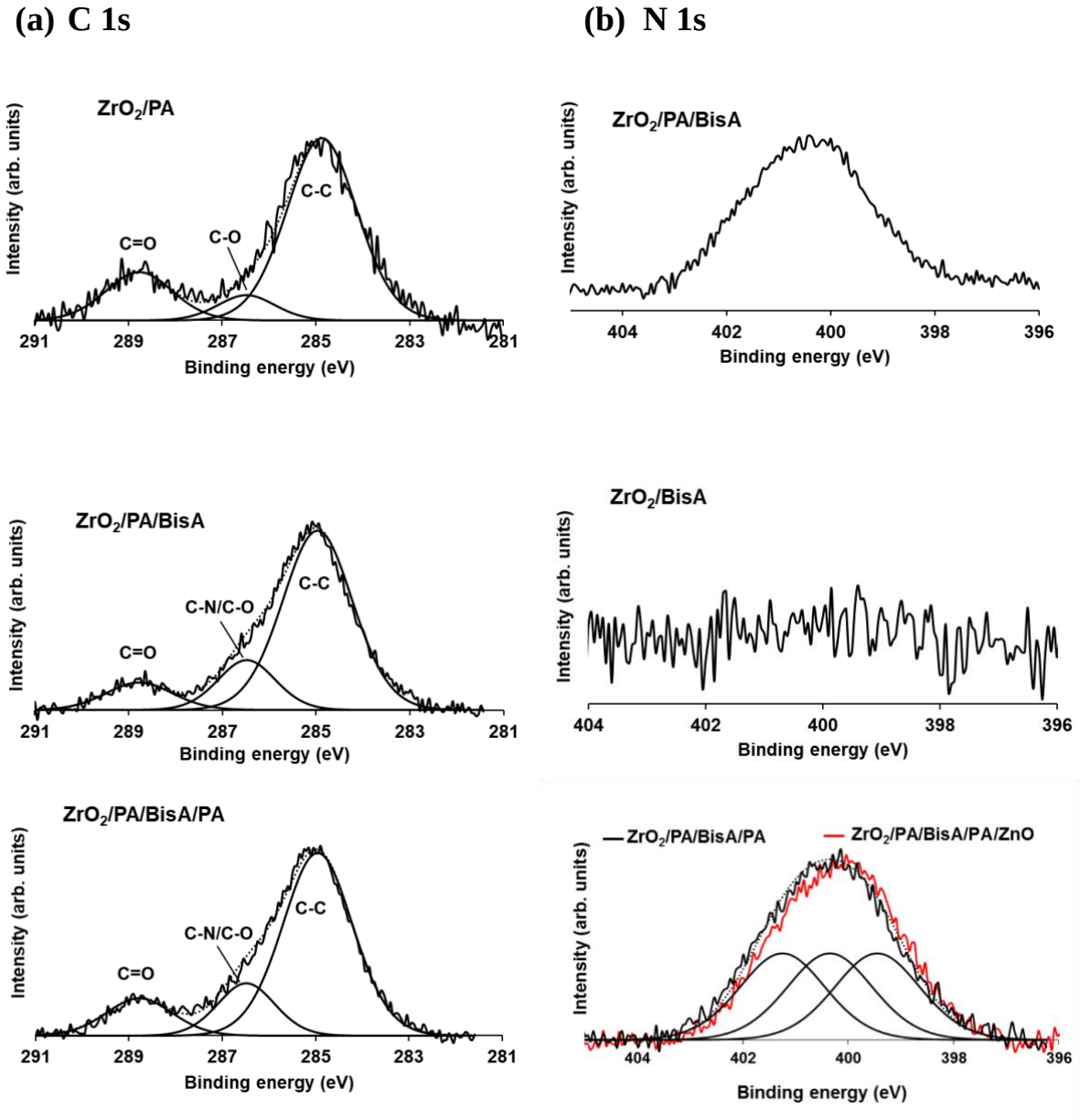

Fig. 2. Normalized XPS spectra of modified ZrO_2 powder substrates under pulsed vapor phase processing conditions, measured *ex situ*: (a) C 1s core-level spectra of **ZrO_2/PA** (top), **ZrO_2/PA/BisA** (middle) and **ZrO_2/PA/BisA/PA** (bottom), (b) N 1s core-level spectra of **ZrO_2/PA/BisA** (top), **ZrO_2/BisA** (middle) and **ZrO_2/PA/BisA/PA** with the superimposed red curve representing **ZrO_2/PA/BisA/PA/ZnO** (bottom). Differently hybridized chemical bonds of C 1s were simply indicated as C-C because the broad peaks do not allow further analysis.

Although ATR-FTIR spectroscopy undoubtedly confirmed the presence of free azide groups, the N 1s XPS spectrum in **Fig. 2b** (top) does not provide a confirmation of azide functionalities in **ZrO_2/PA/BisA**. The reason is that upon longer exposure time the surface-bound $-N_3$ groups undergo X-ray-promoted decomposition in the XPS through a denitrogenation process. This results in the absence of the expected high BE component at

approximately 404 eV, which corresponds to the electron-poor central azide nitrogen (–N=**N**$^{+}$=N^{-}) [29-32]. Previous investigations on XPS-induced denitrogenation of azide propose the formation of imine species as a major decomposition product, generated from unstable nitrene intermediates [29]. Taking this into account, the N 1s peak of **ZrO_2/PA/BisA** seen in **Fig. 2b** (top) most likely stems from the contribution of nitrogen atoms from both triazole moiety and the decomposition product(s). We attempted to provide some evidence for the expected azide degradation in **ZrO_2/PA/BisA** by performing additional XPS experiments in the N 1s region (**Fig. 3**), this time recorded at a pass energy of 50 eV with short exposure times (1, 10 and 20 minutes, respectively). The monitoring of the changes in spectral features was carried out at the same surface spot of the sample. In order to reduce the irradiation damage as much as possible, the duration of one scan was kept at 1 minute. The most critical problem in applying such a low number of scans, especially in the case of ZrO_2 substrate with a low conductivity, is the low signal-to-noise ratio. Nevertheless, the spectra recorded after 1 and 10 minutes show the appearance of a component at a BE of 404.7 eV, which corresponds to the central azide nitrogen in **ZrO_2/PA/BisA**. As expected, the intensity of the peak decreases with increasing exposure time as a result of the decomposition process.

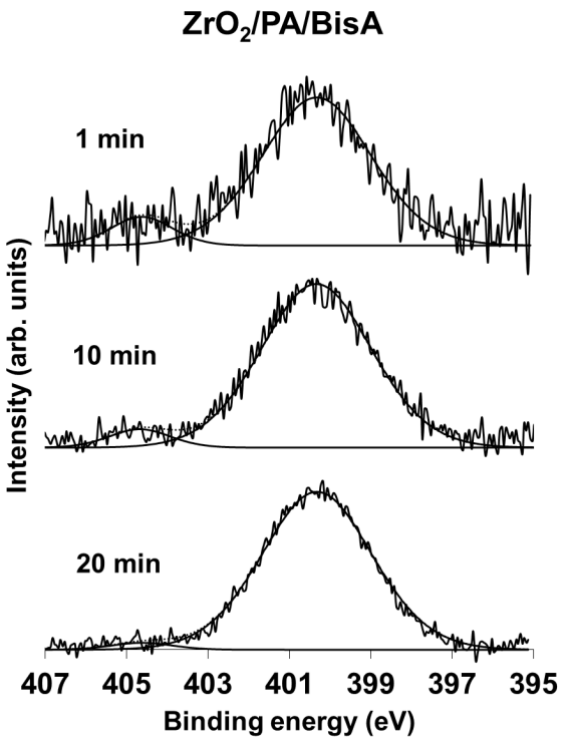

Fig. 3. Monitoring of the decomposition progress of azide nitrogens in **ZrO_2/PA/BisA** by XPS in N 1s spectral region. The spectra were recorded at a pass energy of 50 eV with the indicated exposure times.

The sample **ZrO_2/PA/BisA** was then exposed to PA vapors for the second time in the third ALD processing step. The deconvoluted XPS spectrum of the C 1s region of the obtained hybrid **ZrO_2/PA/BisA/PA** (**Fig. 2a**, bottom) exhibits a relative increase in intensity of C=O when compared to C-N/C-O and C-C signals, thus suggesting a binding of additional PA to the surface, which is also supported by the ATR-FTIR spectra (**Fig. 1**). However, due to adventitious carbon contamination, which affects the survey spectrum of the sample, no conclusions can be drawn regarding the relative yield of the two competitive reactions, i.e.: i) click reaction of the PA alkyne with the pendant -N_3 group, which results in a second triazole moiety with free carboxylic groups (represented by the ratio of C-N/C-O to C=O), and ii) binding of the PA carboxylate directly to newly available zirconia surface sites, leading to free alkyne groups (represented by the ratio of C-C *vs* C=O peak). In the spectrum of the N 1s region (**Fig. 2b**, bottom), the numerical fit of the broad peak centered at a BE around 400 eV reveals the presence of 3 contributions, corresponding to the 3 nitrogen atoms in the triazole rings (401.2 eV, 400.3 eV, and 399.3 eV). The contribution from the decomposition of unreacted azide groups seems not to interfere with the fitting due to the lower content of azide in **ZrO_2/PA/BisA/PA**, as supported by the ATR-FTIR spectrum.

Following the ALD deposition of ZnO on **ZrO_2/PA/BisA/PA**, the XPS spectrum of the ZnO-deposited sample **ZrO_2/PA/BisA/PA/ZnO** showed the appearance of new peaks at 1022.5 and 1046.5 eV representing the Zn 2p core-level (*see* **Fig. S2** in the Supporting material). The N 1s spectrum shows only a marginal change, a slight peak shift towards lower BE, as depicted by the superimposed red curve in **Fig. 2b**, bottom. This feature may indicate a negligible extent of the complexation of zinc ions from Et_2Zn with electron-donating nitrogen atoms in the 1,2,3-triazolyl groups [33, 34]. Namely, as the zinc-triazole coordination is prevalently electrostatic in nature, it is very likely that under ALD conditions the Et_2Zn reversibly desorbs from the two triazole nitrogen sites. Therefore, by combining the results obtained from ATR-FTIR and XPS spectroscopies, we can conclude that the initial surface binding of Et_2Zn to the organic phase in **ZrO_2/PA/BisA/PA** occurs predominantly through a reaction with COOH groups, while the triazole moieties exhibit a low reactivity towards Et_2Zn under the applied processing conditions. These findings are important steps towards understanding the reactivity of various organic functionalities with metal-organic precursors from the gas-phase, which are fundamental for controlling and designing syntheses of hybrid materials by ALD [35].

The investigated multi-step ALD pulsed-vapor phase method is an innovative approach to *in-situ* build functional organic phases on ceramic substrates through consecutive azide-alkyne click reactions. Moreover, the ALD set-up enables an insertion of free carboxylic

functionalities to the surface of the metal oxide without applying invasive oxidation reactions, which are commonly used for the formation of pendant –COOH groups, both in solution and in gas-phase [36-40].

In another approach to prove the presence of terminal carboxylic acid functionalities, we have further examined the stability of **ZrO_2/PA/BisA/PA** in ethanolic dispersions and compared it to virgin ZrO_2 nanopowder. While the latter completely precipitates within the first 20 min, the **ZrO_2/PA/BisA/PA** starts to precipitate after 2 hours only (**Fig. 4**). The higher stability of the latter sample in dispersion is attributed to the organic modification and the free polar -COOH groups that can form more stable H-bonds with ethanol, in contrast to the self-aggregation of Zr-OH that occurs in its pure form.

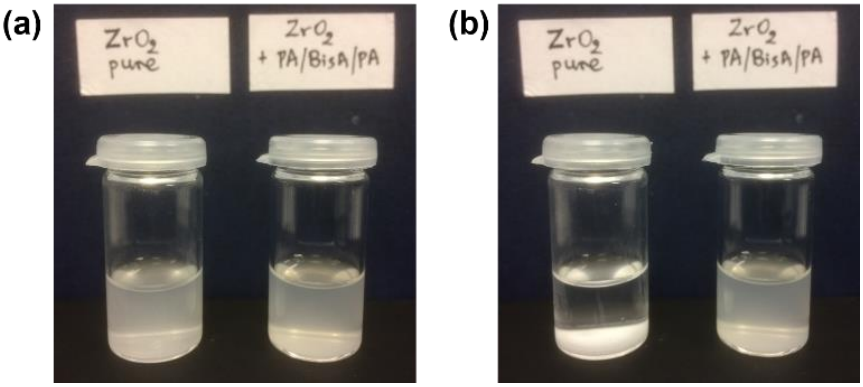

Fig. 4. Photographs of pure ZrO_2 nanopowder (left) and **ZrO_2/PA/BisA/PA** (right) in ethanolic dispersions (solid content 0.4 mg mL^{-1}, sonication of 3 min) (a) immediately after their preparation, and (b) 1.5 hours later.

To evaluate the difference of the vapor phase approach and the most obvious "classical" solution phase functionalization of the ZrO_2 surface using a pre-synthesized organic molecule with the same composition, we investigated the grafting of compound **3**, containing two terminal COOH and two triazole groups, from a 1 mM solution in DMF, on ZrO_2 (**Scheme 2**). The compound was synthesized through a two-step procedure in liquid phase, the second step being a CuAAC click reaction between BisA and an excess of PA (see **Scheme S1** in the Supporting material). After the solvent removal, the obtained product **ZrO_2/3** was subjected to ATR-FTIR and XPS characterizations.

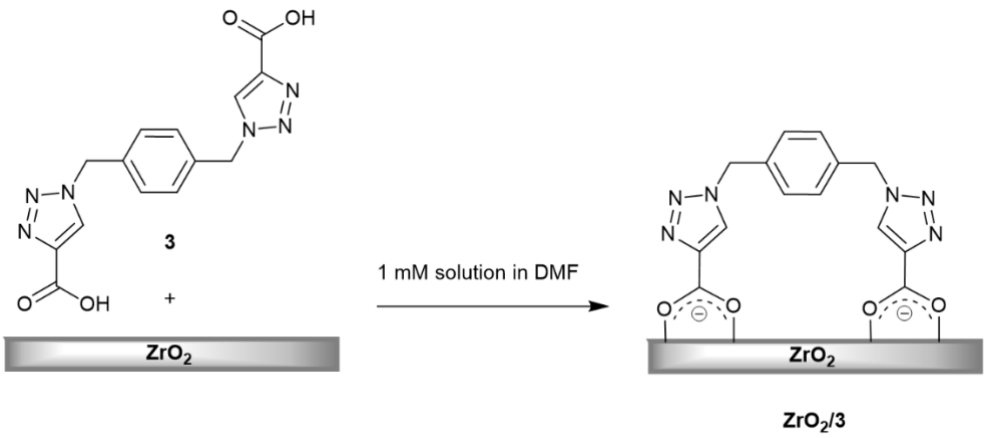

Scheme 2. Surface modification of zirconia by drop casting a 1 mM solution of **3** in DMF onto ZrO_2.

Fig. 5 shows the ATR-FTIR spectrum of **ZrO_2/3** taken in the 1000-2200 cm^{-1} spectral region. The spectra of **3** and **ZrO_2/PA/BisA/PA** are also shown for comparison. Similar to **ZrO_2/PA/BisA/PA**, the triazole moieties in **ZrO_2/3** are represented by C-N and C-H stretching vibrations at 1299 cm^{-1} and at 3137 cm^{-1} (not shown here), respectively, while the presence of an aromatic ring is confirmed by an aromatic C-H in-plane bending at 1045 cm^{-1}. Moreover, coinciding with the spectrum of **3**, the broad peak centered at approximately 1235 cm^{-1} most probably shows overlapping vibrations of N=N and C-O-H moieties. Overall, the similarities between the spectra of ALD- and solution-processed ZrO_2 confirm the presence of the structural elements in both cases, except for the carboxyl functionalities, which can be explained with the spectrum of **3**. The C=O signal of **3** consists of two components: i) an intensive stretching vibration at 1679 cm^{-1}, representing dimeric and/or oligomeric structures resulting from hydrogen bonding between –COOH groups, and ii) a lower-intensity signal at approximately 1710 cm^{-1}, indicating a minor content of free (monomeric) carboxylic groups that do not participate in hydrogen bonding [41]. The latter coincides with the C=O stretching at 1716 cm^{-1} in the ATR-FTIR spectrum of **ZrO_2/PA/BisA/PA**, thus providing additional evidence on the formation of pending COOH groups in the investigated three-step ALD process. After grafting **3** onto the surface of zirconia, the ATR-FTIR spectrum of **ZrO_2/3** shows the appearance of two strong peaks at around 1570 and 1420 cm^{-1} representing asymmetric and symmetric vibrational bands of COO^- groups bound to zirconia, respectively. However, contrary to **ZrO_2/PA/BisA/PA**, the absence of the signal of free COOH suggests that the binding of **3** from the solution occurs through both carboxylic acid functionalities present in the molecule (see **Scheme 2**). Therefore, the increased flexibility of the molecule in a solution-phase, combined with the stabilization through strong ionic bonding with the zirconia surface upon the solvent

removal, lead to a double surface reaction *via* the bent conformation of the molecule. This results in a deactivation of COOH groups for potential post-modification applications. Thus, the control experiment emphasized the advantage of using ALD for the *in-situ* catalyst- and solvent-free generation of functional molecular structures built through stepwise gas-phase click reactions.

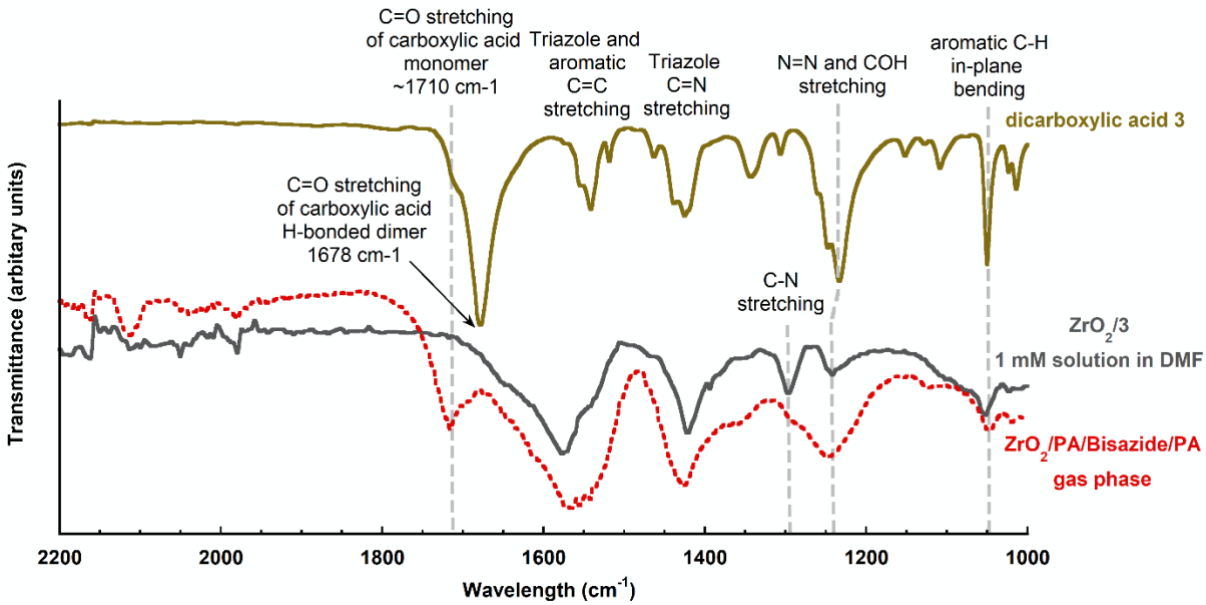

Fig. 5. ATR-FTIR spectra (2200-1000 cm^{-1} region) of zirconia, modified with a solution of dicarboxylic acid (**ZrO_2/3**), compared with the spectrum (dotted line) of the three-step pulsed vapor phase modification (**ZrO_2/PA/BisA/PA**) and the spectrum of free dicarboxylic acid **3**. The spectra of functionalized zirconia are normalized to the Zr-O bands at 745 cm^{-1} and the spectrum of the free dicarboxylic acid **3** is reduced to the same scale.

Fig. 6 shows the XPS spectra of the C 1s and N 1s spectral region of **ZrO_2/3**. The C 1s core level shows the same components as the corresponding spectrum of **ZrO_2/PA/BisA/PA**. The higher relative ratio of the C-C component is attributed to adventitious carbon contamination due to the *ex-situ* preparation/characterization of the sample. Although the broad N 1s peak, representing two triazole moieties of **3** in **ZrO_2/3**, appears to shift slightly to a lower BE, it also exhibits features very similar to the N 1s signal in **ZrO_2/PA/BisA/PA** (superimposed red curve in **Fig. 6**), thus providing an additional evidence for successful click reactions from the gas phase. According to previous investigations, and supported by DFT calculations [23], the cause of the shift of the N 1s peak could be due to the difference in the regioselectivity of the click-reaction.

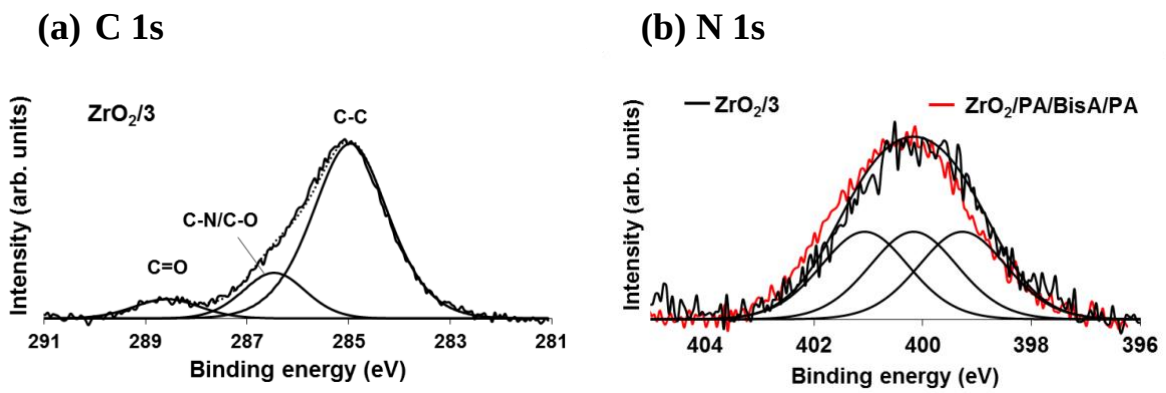

Fig. 6. Normalized XPS spectra of (a) C 1s and (b) N 1s core-levels of surface modified ZrO_2 powder prepared after the addition of a 1 mM solution of **3** (**ZrO_2/3**). Comparison with the gas phase modified substrates (**ZrO_2/PA/BisA/PA**, red line) is shown for N 1s.

The surface coverages of ZrO_2 in **ZrO_2/PA/BisA/PA** and **ZrO_2/3** were evaluated by thermogravimetric analyses (TGA) (*see* **Fig. S3** in the Supporting material). The grafting density (ρ) was calculated with **Eq. (1)** [42], where the wt%(**3**) is the measured weight loss percentage of component 3, wt%(ZrO_2) is the percentage of the zirconia residue, d(ZrO_2) is the density of ZrO_2 (5.68 g/cm^3), NA is the Avogadro constant, V is the averaged volume of a single ZrO_2 particle ($4/3\pi r^3$), S is the surface area per particle ($4\pi r^2$) and M is the molar mass of **3** (328.29 g/mol). For **ZrO_2/PA/BisA/PA** the wt%(**3**) and M were modified correspondingly.

$$\boldsymbol{\rho = \frac{\frac{wt\%(3)}{wt\%(ZrO2)} \text{ x } d(ZrO2)\ x\ V\ x\ NA}{M\ x\ S}} \qquad \textbf{Eq. (1)}$$

The calculated values of the grafting densities in **ZrO_2/PA/BisA/PA** and **ZrO_2/3** are 1.20 and 0.42 molecules per nm^2 of zirconia, respectively. From the obtained results we can see that the gas-phase modification has benefits over the corresponding wet-chemical modification as it allows a much denser packing of the surface with functional molecules.

For the present proof-of-concept study on performing subsequent click-reactions by ALD, we used dry and suspended zirconia powder as substrate. Obviously, the surface coverage of individual nanoparticles in such agglomerated clusters cannot be optimal as the vaporized precursors are unable to bind to surfaces where the particles touch each other. However, for an applied approach this issue can be easily addressed, namely by performing the ALD process in a dynamic reactor, for example a so-called fluidized bed reactor, where the particles are in permanent motion and their mutual contact is minimized.

4. Conclusions

We have developed an *in-situ* three-step pulsed vapor phase organic modification of ZrO_2 based on thermal azide-alkyne click reactions using the ALD processing technique. The investigated automated process consisted on initial gas-phase chemisorption of propiolic acid (PA) to ZrO_2, followed by the formation of a triazole ring through the click-reaction of the PA-modified ZrO_2 with 1,4-bis(azidomethyl)benzene (BisA) vapors and, in the final step, click-coupling of PA to the pendant azide groups with a second dose of PA vapors.

The described process exploits all the advantages of ALD by using a single setup under solvent- and catalyst-free conditions, thus avoiding contamination of the ceramic materials, which can easily occur in solution-based approaches. Moreover, a direct comparison with the wet chemical surface modification with a pre-synthesized dicarboxylic acid revealed an additional advantage of the pulsed vapor phase reactions in enabling a non-invasive introduction of terminal COOH groups. The latter functionalization of the nanomaterial surface can be especially interesting for the development of metal ion capture, enzymatic bio-sensing or bioimaging devices. Similar ALD processes can be also envisaged for the preparation of higher order lattices of organic-inorganic hybrid layers on various structures varying from nanoparticles to thin films. The drawback of the methodology is obviously the need of organic molecules which are sufficiently volatile and thermally stable. However, the possibility to perform sequences of click reactions allows to design a sequential chemical reaction with several smaller molecules in a single process, which, considering that no purification or cleaning is necessary, would still be temporally and economically favorable, particularly in view of the up-scalability of the process by using, for example, a fluidized bed ALD reactor or any other type of powder coating reactor.

Acknowledgment

This work has been mainly supported by Croatian Science Foundation under the project IP-2016-06-3568, and in part by the University of Rijeka under the project uniri-sp-prirod-18-13. The characterization instruments applied in this work were acquired through the European Fund for Regional Development and Ministry of Science, Education and Sports of the Republic of

Croatia under the project Research Infrastructure for Campus-based Laboratories at the University of Rijeka (grant number RC.2.2.06-0001). Mato Knez is grateful for the support by the Spanish Ministry of Economy and Competitiveness (MINECO) [Grant Agreement No. MAT2016-77393-R], including FEDER funds, and the Maria de Maeztu Units of Excellence Programme [grant number MDM-2016-0618].

References

[1] J. M. Vohs, Site Requirements for the Adsorption and Reaction of Oxygenates on Metal Oxide Surfaces, Chem. Rev. 113 (2013) 4136-4163, https://doi.org/10.1021/cr300328u.

[2] S. P. Pujari, L. Scheres, A. T. M. Marcelis, H. Zuilhof, Covalent Surface Modification of Oxide Surfaces, Angew. Chem. Int. Ed. 53 (2014) 2-36, https://doi.org/10.1002/anie.201306709.

[3] V. V. Rostsovsev, L. G. Green, V. V. Fokin, K. B. Sharpless, A stepwise huisgen cycloaddition process: copper(I)-catalyzed regioselective "ligation" of azides and terminal alkynes, Angew. Chem. Int. Ed. 41 (2002) 2596-2599, https://doi.org/10.1002/1521-3773(20020715)41:14<2596:AID-ANIE2596>3.0.CO;2-4.

[4] M. A. White, J. A. Johnson, J. T. Koberstein, N. J. Turro, Toward the Syntheses of Universal Ligands for Metal Oxide Surfaces: Controlling Surface Functionality through Click Chemistry, J. Am. Chem. Soc. 128 (2006) 11356-11357, https://doi.org/10.1021/ja064041s.

[5] L. M. Bishop, J. C. Yeager, X. Chen, J. N. Wheeler, M. D. Torelli, M. C. Benson, S. D. Burke, J. A. Pedersen, R. J. Hamers, A citric acid-derived ligand for modular functionalization of metal oxide surfaces via "click" chemistry, Langmuir 28 (2012) 1322-1329, https://doi.org/10.1021/la204145t.

[6] M. G. Williams, A. V. Teplyakov, Building high-coverage monolayers of covalently bound magnetic nanoparticles, Appl. Surf. Sci. 388 (2016) 461-467.

[7] Y. G. Aronoff, B. Chen, G. Lu, C. Seto, J. Schwartz, S. L. Bernasek, Stabilization of Self-Assembled Monolayers of Carboxylic Acids on Native Oxides of Metals, J. Am. Chem. Soc. 119 (1997) 259-262, https://doi.org/10.1021/ja953848+.

[8] B. H. Lee, M. K. Ryu, S.-Y. Choi, K.-H. Lee, S. Im, M. M. Sung, Rapid Vapor-Phase Fabrication of Organic-Inorganic Hybrid Superlattices with Monolayer Precision, J. Am. Chem. Soc. 129 (2007) 16034-16041, https://doi.org/10.1021/ja075664o.

[9] C. He, R. Janzen, S. Bai, A. V. Teplyakov, ‘Clickable’ Metal Oxide Nanomaterials Surface-Engineered by Gas Phase Covalent Functionalization with Prop-2-ynoic Acid, Chem. Mater. 31 (2019) 2068-2077, https://doi.org/10.1021/acs.chemmater.8b05124.

[10] S. M. George, Atomic Layer Deposition: An Overview, Chem. Rev. 110 (2010) 111-131, https://doi.org/10.1021/cr900056b.

[11] K. Gregorczyk, M. Knez, Hybrid Nanomaterials through Molecular and Atomic Layer Deposition: Top Down, Bottom up, and In-between Approaches to Make and Modify New Materials, Prog. Mater. Sci. 75 (2016) 1-37, https://doi.org/10.1016/j.pmatsci.2015.06.004.

[12] I. Saric, R. Peter, M. Kolympadi Markovic, I. Jelovica Badovinac, C. Rogero, M. Ilyn, M. Knez, G. Ambrožić, Introducing the concept of pulsed vapor phase copper-free surface click-chemistry using the ALD technique, Chem. Commun. 55 (2019) 3109-3112, https://doi.org/10.1039/C9CC00367C.

[13] Y.-h. Li, D. Wang, J. M. Buriak, Molecular Layer Deposition of Thiol−Ene Multilayers on Semiconductor Surfaces, Langmuir 26 (2010) 1232-1238, https://doi.org/10.1021/la902388q.

[14] S. Sommers, J. D. Barnes, The preparation of some organic diazides, J. Am. Chem. Soc. 79 (1957) 3491-3492, https://doi.org/10.1021/ja01570a050.

[15] Z. Hu, M. Khurana, Y. Huang, Y. H Seah. M. Zhang, Z. Guo, D. Zhao, Ionized Zr-MOFs for highly efficient post-combustion CO_2 capture, Chem. Eng. Sci. 124 (2015) 61-69, https://doi.org/10.1016/j.ces.2014.09.032.

[16] S. Yuan, J. Zhang, Z. Yang, S. Tang, B. Liang, S. O. Pehkonen, Click functionalization of poly(glycidyl methacrylate) microspheres with triazole-4-carboxylic acid for the effective adsorption of Pb(II) ions, New J. Chem. 41 (2017) 6475-6488, https://doi.org/10.1039/C7NJ00797C.

[17] M. Yüce, H. Kurt, How to make nanobiosensors: surface modification and characterisation of nanomaterials for biosensing applications, RSC Adv. 7 (2017) 49386-49403, https://doi.org/10.1039/C7RA10479K.

[18] A. Sedlmeier, H. H. Gorris, Surface modification and characterization of photon-upconverting nanoparticles for bioanalytical applications, Chem. Soc. Rev., 44 (2015) 1526-1560, https://doi.org/10.1039/C4CS00186A.

[19] J. R. Thomas, X. Liu and P. J. Hergenrother, Size-specific ligands for RNA hairpin loops, J. Am. Chem. Soc., 127 (2006) 12434-12435, https://doi.org/10.1021/ja051685b.

[20] E. G. Palacios,, G. Juárez-López , A. J. Monhemius, Infrared spectroscopy of metal carboxylates: II. Analysis of Fe(III), Ni and Zn carboxylate solutions, Hydrometallurgy 72 (2004) 139-148, https://doi.org/10.1016/S0304-386X(03)00137-3.

[21] S. Foraita, J. L. Fulton, Y. A. Chase, A. Vjunov, P. Xu, E. Barath, D. M. Camaioni, C. Zhao. J. A. Lercher, Impact of the Oxygen Defects and the Hydrogen Concentration on the Surface of Tetragonal and Monoclinic ZrO_2 on the Reduction Rates of Stearic Acid on Ni/ZrO_2, Chem. Eur. J. 21 (2015) 2423-2434, https://doi.org/10.1002/chem.201405312.

[22] A. A. Jbarah, A. Ihle, K. Banert, R. Holze, The electrosorption of 1,2,3-triazole on gold as studied with surface-enhanced Raman spectroscopy, J. Raman Spectrosc. 37 (2006) 123-131, https://doi.org/10.1002/jrs.1476.

[23] F. Gao, S. Aminane, S. Bai, A. V. Teplyakov, Chemical Protection of Material Morphology: Robust and Gentle Gas-Phase Surface Functionalization of ZnO with Propiolic Acid, Chem. Mater. 29 (2017) 4063-4071, https://doi.org/10.1021/acs.chemmater.7b00747.

[24] A. Nagai, Z. Guo, X. Feng, S. Jin, X. Chen, X. Ding, D. Jiang, Pore surface engineering in covalent organic frameworks, Nat. Commun. 2 (2011) 536, https://doi.org/10.1038/ncomms1542.

[25] M. J. Penelas, G. J. A. A. Soler-Illia, V. Levi, A. V. Bordoni, A. Wolosiuk, Click-based thiol-ene photografting of COOH groups to SiO_2 nanoparticles: Strategies comparison, Colloids Surf. A Physicochem. Eng. Asp. 562 (2019) 61-70, https://doi.org/10.1016/j.colsurfa.2018.11.023.

[26] F. Ragon, B. Campo, Q. Yang, C. Martineau, A. D. Wiersum, A. Lago, V. Guillerm, C. Hemsley, J. F. Eubank, M. Vishnu Varthan, F. Taulelle, P. Horcajada, A. Vimont, P. L. Llewellyn, M. Daturi, S. Devautour-Vinot, G. Maurin, C. Serre, T. Devic, G. Clet, Acid-functionalized UiO-66(Zr) MOFs and their evolution after intra-framework cross-linking: structural features and sorption properties, J. Mater. Chem. A 3 (2015) 3294-3309, https://doi.org/10.1039/C4TA03992K.

[27] K. Barnholt Klepper, O. Nilsen, H. Fjellvåg, Deposition of thin films of organic–inorganic hybrid materials based on aromatic carboxylic acids by atomic layer deposition, Dalton. Trans. 39 (2010) 11628-11635, https://doi.org/10.1039/C0DT00817F.

[28] K. Barnholt Klepper, O. Nilsen, P.-A.Hansen, H. Fjellvåg, Atomic layer deposition of organic-inorganic hybrid materials based on saturated linear carboxylic acids, Dalton. Trans. 40 (2011) 4636-4646, https://doi.org/10.1039/C0DT01716G.

[29] T. Heinrich, C. H.-H. Traulsen, E. Darlatt, S. Richter, J. Poppenberg, N. L. Traulsen, I. Linder, A. Lippitz, P. M. Dietrich, B. Dib, W. E. S. Unger, C. A. Schalley, The versatility of "Click" reactions: Molecular recognition at interfaces, RSC Adv. 4 (2014) 17694-17702, https://doi.org/10.1039/C4RA01730G.

[30] S. Prakash, T. M. Long, J. C. Selby, J. S. Moore, M. A. Shannon, "Click" Modification of Silica Surfaces and Glass Microfluidic Channels, Anal. Chem. 79 (2007) 1661-1667, https://doi.org/10.1021/ac061824n.

[31] G. Zorn, L.-H. Liu, L. Arnadottir, H. Wang, L. J. Gamble, D. G. Castner, M. Yan, X-ray Photoelectron Spectroscopy Investigation of the Nitrogen Species in Photoactive Perfluorophenylazide-Modified Surfaces, J. Phys. Chem. C 118 (2014) 376-383, https://doi.org/10.1021/jp409338y.

[32] A. Saad, M. Abderrabba, M. M. Chehimi, X-ray induced degradation of surface bound azido groups during XPS analysis, Surf. Interface Anal. 49 (2017) 340-344, https://doi.org/10.1002/sia.6113.

[33] B Schulze, U. S. Schubert, Beyond click chemistry – supramolecular interactions of 1,2,3-triazoles, Chem. Soc. Rev. 43 (2014) 2522-2571, https://doi.org/10.1039/C3CS60386E.

[34] J. T. Simmons, J. R. Allen, D. R. Morris, R. J. Clark, C. W. Levenson, M. W. Davidson, L.i Zhu, Integrated and Passive 1,2,3-Triazolyl Groups in Fluorescent Indicators for Zinc(II) Ions – Thermodynamic and Kinetic Evaluations, Inorg. Chem. 52 (2013) 5838-5850, https://doi.org/10.1021/ic302798u.

[35] F. Yang, J. Brede, H. Ablat, M. Abadia, L. Zhang, C. Rogero, S. D. Elliot, M. Knez, Reversible and Irreversible Reactions of Trimethylaluminum with Common Organic Functional Groups as a Model for Molecular Layer Deposition and Vapor Phase Infiltration, Adv. Mater. Interfaces 4 (2017) 1700237, https://doi.org/10.1002/admi.201700237.

[36] L. Keskiväli, M. Putkonen, E. Puhakka, E. Kenttä, J. Kint, R. K. Ramachandran, C. Detavernier, P. Simell, Molecular Layer Deposition Using Ring-Opening Reactions: Molecular Modeling of the Film Growth and the Effects of Hydrogen Peroxide, ACS Omega 3 (2018) 7141-7149, https://doi.org/10.1021/acsomega.8b01301.

[37] L. K. K. Svärd, M. Putkonen, E. Kenttä, T. Sajavaara, F. Krahl, M. Karppinen, K. Van de Kerckhove, C. Detavernier, P. Simell, Molecular Layer Deposition Using Ring-Opening Reactions: Molecular Modeling of the Film Growth and the Effects of Hydrogen Peroxide, Langmuir 33 (2017) 9657-9665, https://doi.org/10.1021/acsomega.8b01301.

[38] V. Muhr, S. Wilhelm, T. Hirsch, O. S. Wolfbeis, Upconversion nanoparticles: from hydrophobic to hydrophilic surfaces, Acc. Chem. Res. 47 (2014) 3481-3493, https://doi.org/10.1021/ar500253g.

[39] H.-P. Zhou, C.-H. Xu, W. Sun, C.-H. Yan, Clean and Flexible Modification Strategy for Carboxyl/Aldehyde-Functionalized Upconversion Nanoparticles and Their Optical Applications, Adv. Funct. Mater. 19 (2009) 3892-3900, https://doi.org/10.1002/adfm.200901458.

[40] A. Sedlmeier, H. H. Gorris, Surface modification and characterization of photon-upconverting nanoparticles for bioanalytical applications, Chem. Soc. Rev. 44 (2015) 1526-1560, https://doi.org/10.1039/C4CS00186A.

[41] A. Martínez-Felipe, A. G. Cook, M. J. Wallage, C. T. Imrie, Hydrogen bonding and liquid crystallinity of low molar mass and polymeric mesogens containing benzoic acids: a variable temperature Fourier transform infrared spectroscopic study, Phase Transitions 87 (2014) 1191-1210, https://doi.org/10.1080/01411594.2014.900556.

[42] D. N. Benoit, H. Zhu, M. H. Lilierose, R. A. Verm, N. Ali, A. N. Morrison, J. D. Fortner, C. Avendano, V. L. Colvin, Measuring the Grafting Density of Nanoparticles in Solution by Analytical Ultracentrifugation and Total Organic Carbon Analysis, Anal Chem. 84 (2012) 9238–9245.

Figure captions:

Scheme 1. Pulsed vapor phase surface modification process of zirconia in three steps using propiolic acid **(1)** (PA) and 1,4-bis(azidomethyl)benzene **(2)** (BisA) as organic precursors. Note that the growth does not involve cross-linking of the molecules.

Fig. 1. ATR-FTIR spectra of: (a) **ZrO_2/PA**, **ZrO_2/PA/BisA**, **ZrO_2/PA/BisA/PA** and **ZrO_2/PA/BisA/PA/ZnO** in the 2200-1000 cm^{-1} region (the magnification around 2100 cm^{-1} shows the characteristic peaks of alkyne and azide functionalities); and (b) representative vibration bands of **ZrO_2/PA**, **ZrO_2/PA/BisA**, **ZrO_2/PA/BisA/PA** in the 3400-3000 cm^{-1} region. All spectra are normalized to the Zr-O band at 745 cm^{-1}.

Fig. 2. Normalized XPS spectra of modified ZrO_2 powder substrates under pulsed vapor phase processing conditions, measured *ex situ*: (a) C 1s core-level spectra of **ZrO_2/PA** (top), **ZrO_2/PA/BisA** (middle) and **ZrO_2/PA/BisA/PA** (bottom), (b) N 1s core-level spectra of **ZrO_2/PA/BisA** (top), **ZrO_2/BisA** (middle) and **ZrO_2/PA/BisA/PA** with the superimposed red curve representing **ZrO_2/PA/BisA/PA/ZnO** (bottom). Differently hybridized chemical bonds of C 1s were simply indicated as C-C because the broad peaks do not allow further analysis.

Fig. 3. Monitoring of the decomposition progress of azide nitrogens in **ZrO_2/PA/BisA** by XPS in N 1s spectral region. The spectra were recorded at a pass energy of 50 eV with the indicated exposure times.

Fig. 4. Photographs of pure ZrO_2 nanopowder (left) and **ZrO_2/PA/BisA/PA** (right) in ethanolic dispersions (solid content 0.4 mg mL^{-1}, sonication of 3 min) (a) immediately after their preparation, and (b) 1.5 hours later.

Scheme 2. Surface modification of zirconia by drop casting a 1 mM solution of **3** in DMF onto ZrO_2.

Fig. 5. ATR-FTIR spectra (2200-1000 cm^{-1} region) of zirconia, modified with a solution of dicarboxylic acid (**ZrO_2/3**), compared with the spectrum (dotted line) of the three-step pulsed vapor phase modification (**ZrO_2/PA/BisA/PA**) and the spectrum of free dicarboxylic acid **3**. The spectra of functionalized zirconia are normalized to the Zr-O bands at 745 cm^{-1} and the spectrum of the free dicarboxylic acid **3** is reduced to the same scale.

Fig. 6. Normalized XPS spectra of (a) C 1s and (b) N 1s core-levels of surface modified ZrO_2 powder prepared after the addition of a 1 mM solution of **3** (**ZrO_2/3**). Comparison with the gas phase modified substrates (**ZrO_2/PA/BisA/PA**, red line) is shown for N 1s.